International Journal of GEOMATE, June, 2025 Vol.28, Issue 130, pp.1-16
ISSN: 2186-2982 (P), 2186-2990 (O), Japan, DOI: https://doi.org/10.21660/2025.130.4757
Geotechnique, Construction Materials and Environment

3D SUBSURFACE MODELING OF GREATER BEIRUT: INTEGRATING GEOTECHNICAL AND GEOPHYSICAL DATA FOR SEISMIC HAZARD

*Marwa Safa[1,2], Etienne Bertrand[1] and Marleine Brax[2]

[1]GERS-SRO, Gustave Eiffel University, France; [2]CNRS-L, National Center for Geophysics, Lebanon

*Corresponding Author, Received: 09 Oct. 2024, Revised: 13 Feb. 2025, Accepted: 16 Feb. 2025

ABSTRACT: Lebanon's complex tectonic setting has historically caused earthquakes exceeding magnitude 7. Beirut metropolis, Lebanon's economic center, is particularly exposed to seismic hazard due to its proximity to active faults and diverse lithological formations. The subsoil characteristics lead to high ground motion spatial variability with significant seismic amplification. Traditional 1D and 2D models are insufficient to capture the complex effects of bedrock topography, sediment layers, and seismic wave propagation, making the development of a 3D model necessary. In this study, we developed the first simplified 3D subsurface model of Greater Beirut, incorporating data from approximately 500 geotechnical boreholes, 700 H/V spectral ratio measurements, and existing geological studies. The model reveals significant variations in Quaternary sediment thickness, with deposits exceeding 70 meters in the Borj Hammoud area and outcropping rocks in Ras Beirut and Achrafieh. Shear wave velocity averages 300 m/s, enabling the estimation of fundamental resonance frequencies, which range from 0.5 Hz in deep basins to over 10 Hz in rocky zones. By addressing data gaps in southern Beirut using advanced interpolation and machine learning techniques, this model establishes a foundation for future numerical simulations, aiding in seismic hazard assessment and urban planning.

Keywords: Greater Beirut, 3D Geotechnical Model, Seismic Hazard Assessment, Shear Wave Velocity

1. INTRODUCTION

The devastating earthquake in Turkey in February 2023 has underscored the urgent need to reassess seismic risk in Lebanon, particularly in Greater Beirut. Seismic ground motion poses significant challenges to urban environments, requiring accurate predictions to improve earthquake safety and resilience. Historical earthquakes, such as the 2011 Tohoku earthquake in Japan, demonstrated how local geological conditions amplify seismic ground motion, emphasizing the importance of detailed site response analyses to quantify amplification and evaluate surface-subsurface motion interactions [1].

Traditional seismic response analyses often utilize 1D wave propagation models, which assume vertically propagating waves through horizontally stratified layers [2]. While these models are effective for basic assessments, they fall short in accounting for inclined layers, lateral heterogeneities, and complex subsurface geometries, as demonstrated in studies from Japan and California [3-6]. 2D models offer improvements by incorporating horizontal variations in material properties and geometry, enabling the analysis of wave trapping and topographic effects [7-8]. However, they still oversimplify seismic wave interactions by neglecting multi-directional propagation, particularly in sedimentary basins. Basins amplify seismic ground motion through two mechanisms: basin reverberation effects caused by trapped wave energy and basin-edge effects driven by resonance and constructive interference of surface waves [9-11]. Studies of the Grenoble Valley [12] and Seattle Basin [13] have shown that 3D models can capture prolonged shaking and higher amplitudes compared to 2D models.

Greater Beirut's unique tectonic and lithological features, including steep bedrock slopes and heterogeneous sediments, require the adoption of 3D modeling to accurately simulate seismic wave interactions. In addition to amplifying seismic ground motion, the sedimentary basins in the region pose risks of secondary hazards, such as liquefaction during earthquakes. For example, areas like Borj Hammoud, characterized by shallow water tables at depths of approximately 5 meters, are particularly susceptible to liquefaction [14].

Globally, 3D modeling has been successfully used to address seismic hazards. Notable examples include the high-resolution 3D model of Rieti, Italy, which supported seismic response studies; the Nola logistic plant in southern Italy, where complex subsurface conditions were modeled for geotechnical design; and Aachen, Germany, where 3D modeling improved insights into subsurface impacts on urban infrastructure [15-17]. These projects highlight the broader significance of 3D modeling in urban seismic risk assessments while underscoring the need to adapt such approaches to the specific challenges of Greater Beirut.

This study aims to develop a practical 3D geotechnical model of Greater Beirut by combining,

geological, geotechnical, and geophysical data. The model will serve as a foundation for 3D numerical simulations to assess site effects, improving seismic risk evaluations and contributing to the development of resilient urban infrastructure in the region.

2. RESEARCH SIGNIFICANCE

The significance of this research lies in its contribution to understanding seismic hazards in Greater Beirut, a region with complex tectonic and lithological features. By developing the first 3D geotechnical model of the area, the study provides essential tools to accurately assess site effects and spatial ground motion variability. Overcoming the limitations of traditional 1D and 2D approaches, the model serves as a foundation for future numerical simulations, which will enhance seismic risk assessments, guide urban planning, and strengthen the resilience of this densely populated and economically vital region.

3. GREATER BEIRUT GEOLOGICAL, GEOTECHNICAL, AND SEISMOLOGICAL CONTEXT

Beirut, the capital of Lebanon, is situated in a geologically diverse and seismically active region. The city's geological landscape includes formations such as alluvial sands, cemented dune materials (Ramleh), and limestone outcrops, shaped by both natural processes and human activities. Urban expansion has significantly altered these formations, particularly in coastal areas where land reclamation and construction have modified the natural sediment structure [18-19].

Lebanon's position on the Levant Fault System, extending from the Gulf of Aqaba to Turkey, underscores its seismic exposition. This system includes the Roum, Yammouneh, and Rachaya - Serghaya strike-slip faults, located 15 km, 25 km and 50 km from Beirut, respectively, which are all capable of generating large earthquakes. These active faults, part of the Levant Fault System, are influenced by compressional forces, local tectonic movements, and the restraining bend of the fault system, which affects the Mount Lebanon region. This leads to thrust faulting, folding, and uplift, which are reflected in significant elevation variations in the bedrock. The Mount-Lebanon Thrust (MLT) and other minor faults closer to the city contribute to historical and recent shocks (Fig.1). The (MLT) has been linked to significant historical earthquakes, such as the 551 A.D. event with a magnitude of 7.5, which caused widespread damage and a tsunami, resulting in over 30,000 casualties [20-22]. Recent studies confirm the ongoing seismic hazard in Beirut, with a probabilistic seismic hazard assessment indicating a Peak Ground Acceleration (PGA) of up to 0.45g at the 84th percentile [23].

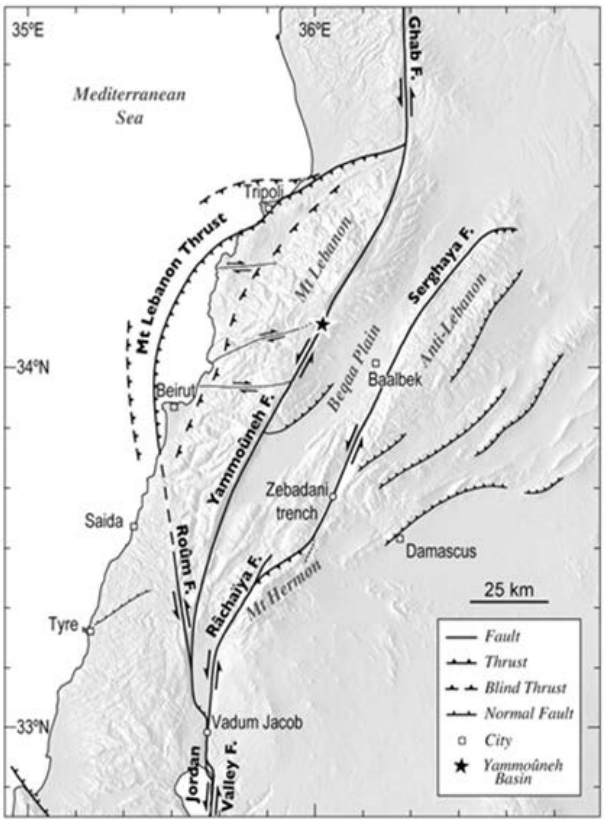

Fig.1 Map of the Levant Fault System showing the major tectonic features highlighting key structures influencing seismic activity in the region [20].

Significant advancements in geophysical investigations have deepened our understanding of Beirut's subsoil characteristics and seismic response. Brax [24] identified fundamental frequencies in the region, revealing areas of significant ground motion amplification, particularly in zones with deep sedimentary deposits as illustrated in Fig. 2. Furthermore, Salloum [25] utilized combined geotechnical and geophysical methods to create 2D subsurface models, near the river of Beirut, further highlighting the spatial variability of alluvial layers.

However, previous studies have been limited in scope, often confined to the municipal boundaries of Beirut or slightly beyond. This narrow focus introduces uncertainty by neglecting the 3D effects essential for understanding seismic response. Our study expands this scope to encompass the GB area as represented in the white rectangle border of Fig.3, seeking to overcome the limitations of 1D and 2D models by developing a comprehensive 3D geotechnical model.

This model will allow to better capture interaction between the seismic waves and the geological structures, such as sedimentary basins, which are prevalent in the Beirut area.

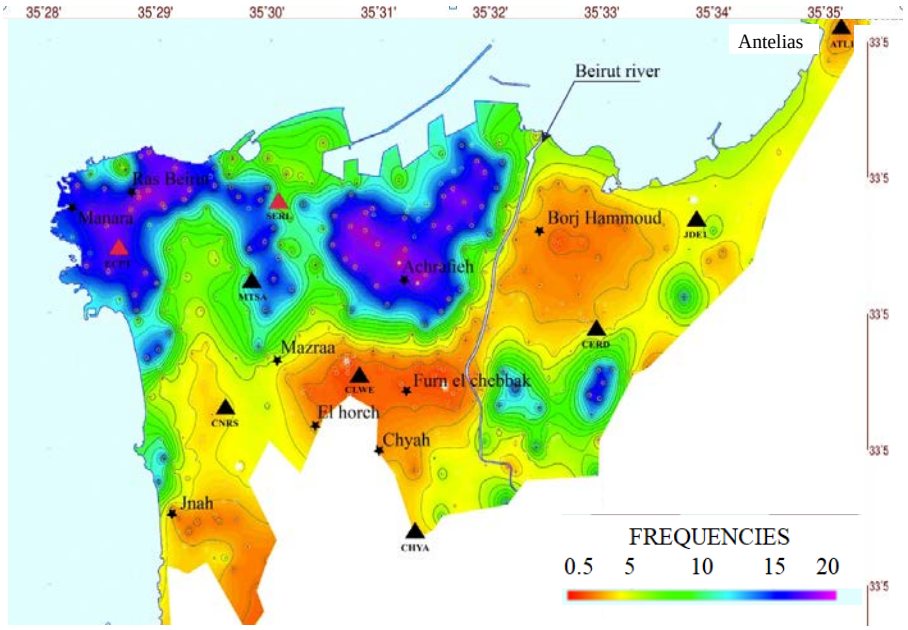

Fig. 2 Interpolated map of fundamental frequencies in Beirut. Frequency (Hz), with reference stations indicated by red triangles, after [24].

The white rectangle in Fig.3 outlines the extended study area, which includes sedimentary zones (brown), Beirut's municipal boundaries (blue), and outcropping rock (white). The hatched light brown area indicates discrepancies between the geological map and the background (Google Earth Pro), primarily due to reclaimed land for ports and the airport, as well as potential inaccuracies in the Dubertret map. It is important to note that the port and airport extensions into the sea are not considered in this model.

Fig.3 Study area overview, showing geological and urban boundaries.

4. DATABASE CONSTRUCTION

4.1 Data sources

Building an accurate 3D geotechnical model requires the integration of various data sources, each contributing as unique insights into the subsurface conditions of GB. Results from [24] revealed minimal variability in shear wave velocity *(Vs)* throughout the Quaternary sediments in the area. Thus, the primary objective of the proposed GB model is to accurately localize the transition between the Quaternary sediments and the underlying bedrock. This model simplifies the subsurface into two primary layers: sediments overlying bedrock, which is the main characteristics influencing seismic site effects.

4.1.1 Topographical and Bathymetric Data

We utilized a detailed 10x10m Digital Elevation Model (DEM) from the National Center for Remote Sensing (CNRS Lebanon) to accurately represent the terrain, excluding building heights for greater precision. Additionally, a bathymetric map of the Mediterranean Sea was incorporated, sourced from GEBCO's global bathymetry grids (GEBCO Compilation Group, 2022). These high-resolution DEMs are crucial for refining the model's terrain representation, thereby improving its capability to predict geological and geotechnical behaviors [27].

4.1.2 Geological Data

To complement our topographical data, we integrated a geo-referenced version of Dubertret's 1944 geological map [28]. The geological map was aligned with the DEM using QGIS software (Version 3.30's - Hertogenbosch), ensuring the consistency between geological and topographical features. This alignment involved careful overlaying and correction of any spatial mismatches, which is essential for accurately representing the geological context within our model [29].

4.1.3 Borehole Data Collection

A total of 594 borehole logs were compiled from various sources, including previous research studies and newly gathered data. Specifically, we incorporated approximately 80 boreholes from [30], 200 from CNRS-Lebanon, and 8 from [25]. The remaining boreholes were newly collected as part of this work. While no new drilling was conducted, significant effort was made to gather and compile existing borehole data, providing detailed lithological descriptions and direct observations of the subsurface. All data were geo-referenced using the UTM36N coordinate system within QGIS.

4.1.4 Geophysical Data

To enhance our geotechnical data, we incorporated 615 ambient vibration measurements from [24,26], supplemented by additional measurements conducted during a campaign in January 2023. These geophysical data are particularly valuable in regions with sparse borehole data, offering cost-effective and time-efficient visions into subsurface conditions. The fundamental resonance frequency, determined by the H/V spectral ratio method [31], provides an estimate of sediment thickness when paired with average shear wave velocity values. Recent research highlights how the HVSR method has become a valuable tool for assessing local seismic responses, mapping sediment thickness, and understanding subsurface layering. Its effectiveness has been demonstrated in diverse environments, from densely populated urban areas like Semarang, Indonesia, to crucial infrastructure zones such as Yogyakarta International Airport, where it plays a key role in identifying seismic amplification risks [32-33].

4.2 Database improvement

The boreholes collected here are predominantly located in the northern part of GB, as illustrated in Fig.4. These boreholes were sourced from various companies and laboratories, each with potentially different methodologies and standards, leading to significant inconsistencies in the data.

4.2.1 Inconsistencies in Lithological Descriptions

A data cleaning process was essential due to inconsistencies in the quality and reliability of borehole logs. Variability arose from discrepancies in sediment terminology, testing methods, and Standard Penetration Test (SPT) values. The data were collected from different sources, each using different methodologies and standards for sediment classification and testing, leading to variability in the descriptions of similar stratigraphic horizons. This variability complicated the comparison of geotechnical reports, suggesting that localized geological conditions could significantly impact stratigraphic continuity. Additionally, the borehole data revealed the presence of different types of bedrock across Greater Beirut. To maintain the model's simplicity and focus, we established a clear definition of bedrock based on borehole reports and Standard Penetration Test (SPT) values. In our classification, layers with SPT values indicating refusal were identified as bedrock, while all other values were considered sediments. This approach allowed us to systematically differentiate between Quaternary sediments. Consequently, weathered or transitional bedrock layers were also classified as bedrock, as we did not distinguish between different types of rock formations, concentrating instead on the main competent bedrock.

4.2.2 Data Location Uncertainty

Another critical challenge was the uncertainty regarding the exact positions of some boreholes. Inaccurate borehole positioning could lead to erroneous interpretations of the geological context, further complicating the analysis and integration of the data. These data have been thus removed from the database.

4.2.3 Outcome of Data Cleaning

Through a thorough data cleaning process, the initial dataset of 594 boreholes was refined to 440, with 64% of these reaching the engineering bedrock. The database thus consists of 284 boreholes that reached the bedrock, 156 boreholes that did not reach it, and 469 H/V measurement points. In addition, 533 control points from the geological map, representing the surface transition between sedimentary soils and bedrock, are included as virtual boreholes (Fig.4). Most boreholes that reached the bedrock are concentrated in areas with a thin sedimentary layer, particularly around rock outcrops in the northern part of the study area (notably Ashrafieh and Ras Beirut). The southern half of the study area, however, lacks sufficient data.

4.3 Sediment Shear Wave Velocity and Thickness Estimation

To estimate the average shear wave velocity *(Vs)* of the sedimentary layer across the entire 10x12 km model area, we employ a combination of geophysical data (H/V measurements) and geotechnical data (borehole reaching bedrock). Assuming a tabular hypothesis and vertically propagating seismic waves, the relationship between the fundamental resonance frequency *(f_0)*, sediment thickness *(EPS)*, and shear wave velocity *(Vs)* is defined by the quarter wavelength approach after Nakamura [34]:

$$f_0 = \frac{Vs}{4.EPS} \quad (1)$$

For this analysis, H/V measurement and borehole

pairs located within 100 meters of each other were included. The scatter plot of resonance frequency *(f_0)* versus sediment thickness *(EPS)* is overlaid with theoretical curves for a median shear wave velocity *(Vs_m)* of 300 m/s, with ranges extending from 165 m/s (16th percentile) to 477 m/s (84th percentile). The histogram highlights the distribution of *Vs* values derived using this approach, with a median *Vs* of 300 m/s (Fig. 5).

5. BEDROCK - SEDIMENT INTERFACE INTERPOLATION STRATEGY

We select suitable interpolation variables and methods to enhance the reliability of bedrock geometry models in the Greater Beirut region. By carefully considering factors such as data distribution and the effectiveness of various interpolation techniques, our goal is to produce accurate and dependable bedrock elevation estimates from the available data.

5.1. Interpolation Variables Selection

Selecting the correct interpolation variable is crucial for accurate bedrock geometry estimation. We compared two potential variables: sediment thickness *(EPS)* and bedrock altitude (elevation above sea level, *ZZ_EPS*). Bedrock altitude is computed as the difference between the digital elevation model (DEM) and *EPS*. The density curve in Fig. 6 illustrates the distributions of these two variables. As shown in Fig. 6, the distribution of bedrock elevation *(ZZ_EPS)* is closer to a normal distribution (red curve) compared to sediment thickness *(EPS)* (blue curve). A normal distribution is desirable because it tends to produce stable and consistent interpolation results, minimizing the risk of artifacts or extreme values that could distort the model. This observation led us to select *ZZ_EPS* as the interpolation variable, ensuring more accurate and dependable bedrock elevation estimations.

5.2 Interpolation Methods

Choosing an efficient interpolation method is essential for constructing a continuous surface of bedrock topography. We evaluated several interpolation methods, with a focus on Triangulated Irregular Network (TIN) and Ordinary Kriging (OK), which have both been used in previous studies for their effectiveness in bedrock elevation estimation.

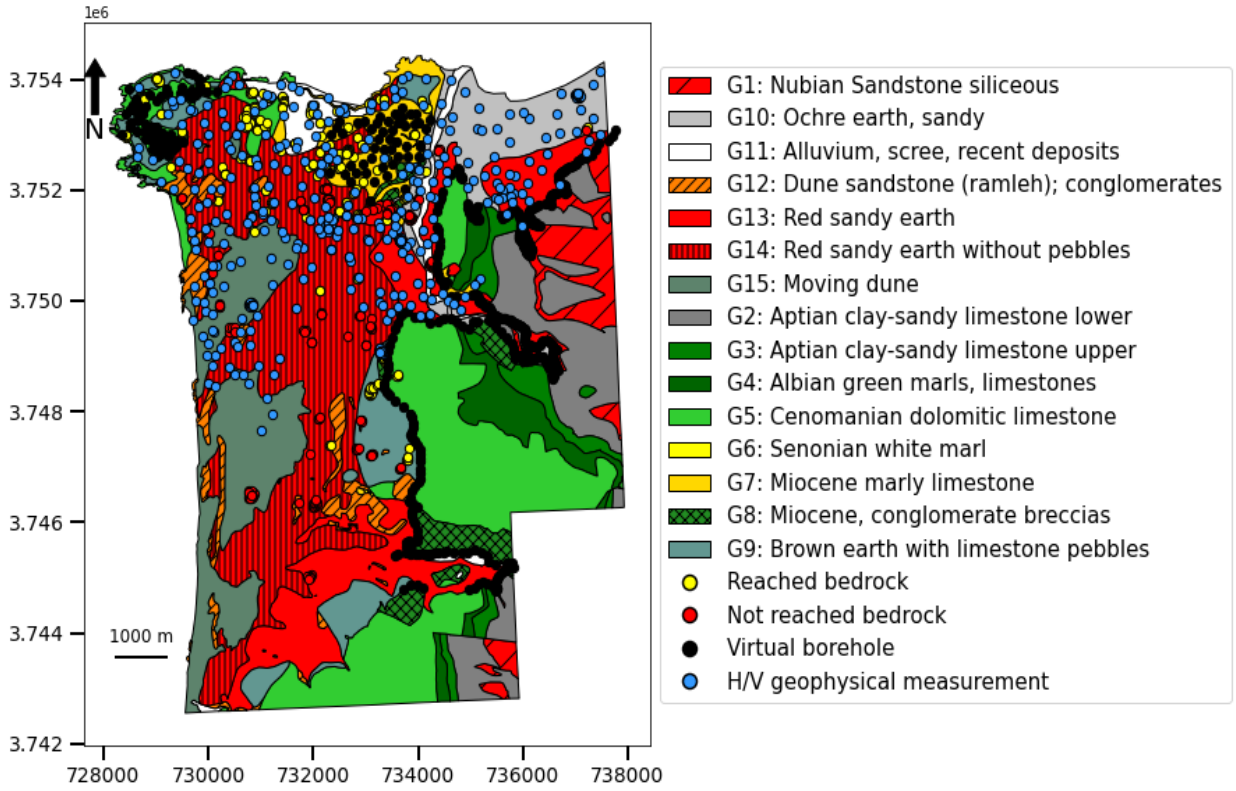

Fig.4 Geological map of Greater Beirut after Dubertret [28], showing borehole locations. Yellow markers indicate boreholes that reached the bedrock, red markers denote boreholes that did not, black markers represent virtual boreholes, and light blue dots correspond to H/V geophysical measurement sites.

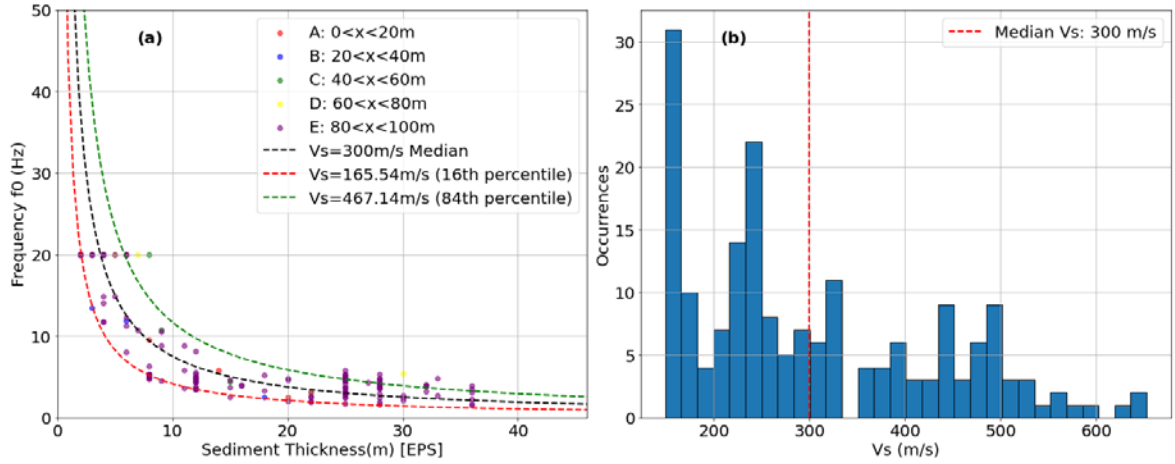

Fig. 5 (a) Scatter plot of resonance frequency *(f_0)* versus sediment thickness *(EPS)* with theoretical curves. (b) Histogram of *Vs* values showing a median of 300 m/s.

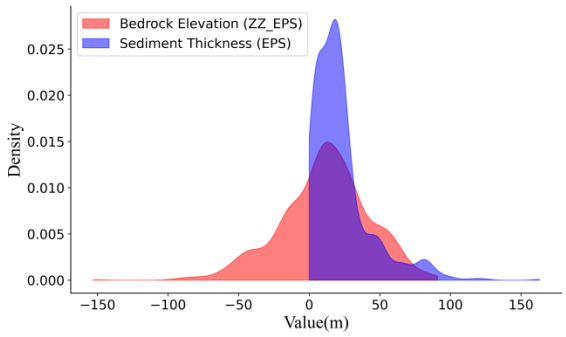

Fig. 6 Density curves comparing bedrock elevation *(ZZ_EPS)* and sediment thickness *(EPS)*.

TIN is well-suited for capturing geometric characteristics of earth surfaces, particularly in terrain and subsurface modeling [35]. On the other hand, Ordinary Kriging (OK) is known for its robustness in handling complex spatial structures, offering precise sediment thickness and bedrock depth estimations. The geostatistical nature of OK, leveraging variograms or semi-variograms, is particularly effective for datasets with non-uniformly clustered data points, allowing statistical and spatial distributions to be considered while generating an uncertainty grid for interpolation accuracy [36,39].

To optimize Ordinary Kriging (OK) for this study, we adjusted the variogram parameters, selecting a lag distance of 100m to ensure stable semivariance calculations based on the dataset distribution. The maximum interpolation distance was set between 5000m and 6000m. This choice is particularly relevant in the central part of the model (between latitudes 3.746 and 3.75 x 10^6), where the distance from the coast to the mountains varies between 4000m and 5000m. As shown in Fig.4, this region consists entirely of different types of Quaternary sediments, which are expected to be spatially correlated, justifying the 5000 m interpolation distance.

However, the study area exhibits high geological heterogeneity, particularly in the northern part of the model (between latitudes 3.752 and 3.754), where the bedrock alternates between shallow coastal outcrops, Quaternary sediments, and deeper deposits towards the east. These transitions, occurring approximately every 2500m, introduce the variability in the variogram and affect its spherical fit beyond 3000m distance (Fig. 7). We retain them intentionally to preserve the broader geological trends of the area. This step of controlling and quantifying interpolation parameters makes it more suitable than deterministic approaches, which rely solely on geometric relationships and lack the ability to account for spatial correlation.

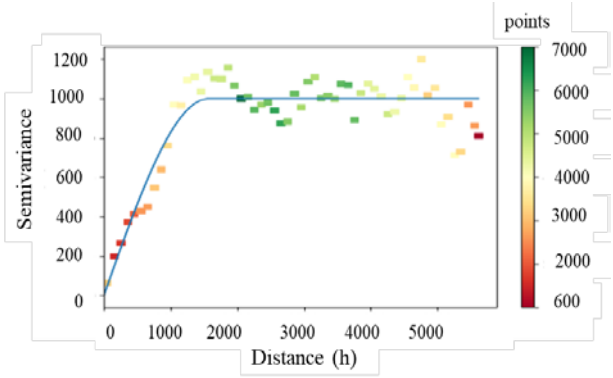

Fig. 7 Isotropic variogram fitted with a spherical model, illustrating the spatial correlation structure of the dataset

5.3 Detrending Consideration

Another important dimension in the OK process is the consideration of detrending. It is well-established in previous geotechnical studies that

spatial trend analysis often serves as a precursor to interpolation techniques. Numerous studies emphasize the synergy of detrending and Kriging, underscoring their efficacy in capturing site-specific spatial correlations, discerning anisotropy, and reducing interpolation errors [40].

Data analysis for Greater Beirut, illustrated in scatter plots of ZZ_EPS against East-West (XX) and North-South (YY) directions, uncovers complex geological trends across the region's varied landscape (Fig. 8). In the East-West direction scatter plot, a dispersed clustering of data points suggests variability that might reflect a complex interplay of geological formations rather than following a clear or simple pattern. This broad scatter indicates that geological factors influencing *ZZ_EPS* values are not linearly correlated with Longitude, implying heterogeneous conditions that would not benefit from a simple detrending approach. Similarly, the North-South direction scatter plot does not reveal an obvious directional trend, with data points forming a broad, diffuse band across the graph. This absence of a clear trend related to the Latitude supports the view that geological variations are multifaceted and not easily captured by a single linear trend at the scale of our model. Therefore, detrending the dataset could oversimplify the underlying geological processes, leading to potential loss of valuable bedrock depth spatial variability information.

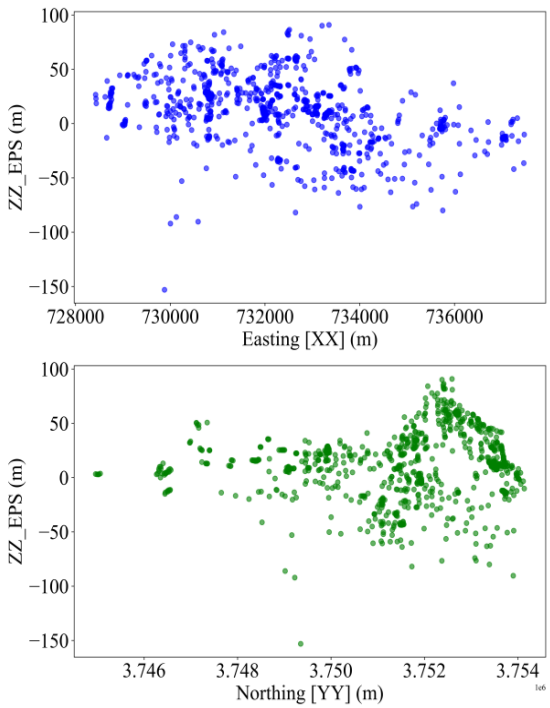

Fig. 8 Scatter plots of *ZZ_EPS* against East-West (XX) and North-South (YY) directions, highlighting dispersed data points and the absence of distinct linear trends.

While at a smaller scale some areas within Beirut might exhibit localized trends warranting detrending, the research scope encompasses the broader city area, mixing different geological units. The primary objective is not a granular examination but a metropolitan-wide analysis. Thus, applying Kriging directly to the dataset without prior detrending ensures the preservation of the spatial variability inherent to Beirut's multifaceted geological conditions, ensuring the results remain both representative and accurate [41].

5.4 Cross-Validation and Model Validation

To evaluate the reliability of the interpolation model, we performed cross-validation by splitting the dataset into training and testing sets. This method allowed us to identify potential issues like underfitting or overfitting and ensured accurate predictions. Model performance was assessed using the root mean square error (RMSE) and determination coefficient (R^2). The results indicate that interpolating bedrock elevation *(ZZ_EPS)* outperforms sediment thickness *(EPS)*, with lower RMSE and higher R^2 values. The tighter clustering of data points around the trendline for bedrock elevation highlights its stronger correlation and superior predictive accuracy compared to sediment thickness (Fig. 9).

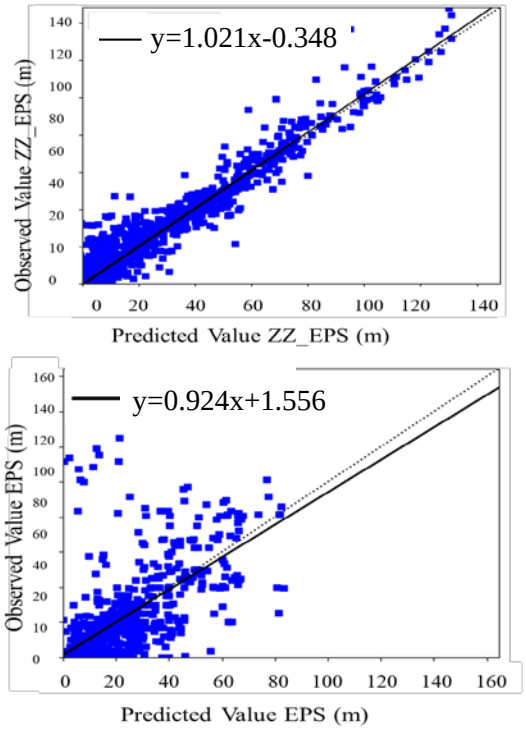

Fig. 9 Validation results of the interpolation's performance for (a) sediment thickness *(EPS)* and (b) bedrock elevation *(ZZ_EPS)*.

6. ADAPTED MODELING METHODOLOGY

We develop an adapted methodology to develop a simplified 3D model of bedrock elevation for Greater Beirut. This approach particularly integrates both type of boreholes those that reach bedrock and those that do not, using an iterative process to refine the model progressively.

6.1 Iterative Modeling Approach

To construct an accurate 3D model, we implemented an iterative modeling strategy, beginning with interpolating the bedrock surface using borehole data and geophysical H/V measurements, which were converted into bedrock depth values. The initial interpolation provides a preliminary bedrock surface model. This model is then compared with sediment depths from boreholes that do not reach bedrock, which are used to adjust regions where the interpolated values are inconsistent with observed data, whether due to insufficient data coverage or mismatches with HVSR-derived sediment thickness values. If discrepancies exceed known geological constraints, such as maximum bedrock elevation, local corrections are applied to ensure consistency.

The process is repeated iteratively, refining the model until convergence is achieved, meaning further iterations result in negligible changes to the bedrock surface. This refinement improves the model's accuracy and reduces uncertainties, ensuring it aligns closely with geological realities. To account for transitions between sediment-covered areas and exposed bedrock, virtual boreholes with zero sediment thickness are introduced at bedrock outcrops, adding boundary conditions that maintain geological authenticity (Fig. 10).

The comparison step in the iterative modeling process involves evaluating the predicted bedrock surface against minimum sediment depths from boreholes that do not reach bedrock. This step identifies areas where the initial interpolation might deviate from observed data. For example, as shown in Fig. 11, three boreholes (A, C, and E) reach bedrock, while two boreholes (B and D) do not. Initially, the sediment/bedrock interface between A and C is modeled as a dashed line without considering borehole B. However, borehole B imposes a constraint requiring the bedrock depth to be larger. Incorporating this constraint results in a more accurate interface, represented by the red curve. In contrast, borehole D does not impose a constraint, and the bedrock topography in that area remains similar to the initial iteration. This iterative refinement ensures the final bedrock model aligns with both geological constraints and observed data variability (Fig. 11).

6.2 Extension of the Model to the South

To extend our bedrock elevation model into the southern part of GB, where data is almost non existant, we employ a Random Forest (RF) machine learning approach. RF is well-suited for this task due to its robustness against overfitting and its ability to handle complex, non-linear relationships in spatial data.

6.2.1 Random Forest Overview

Random Forest (RF) is an ensemble learning method that improves model accuracy and robustness by combining predictions from multiple decision trees. This approach reduces the risk of overfitting—a common issue where models perform well on training data but poorly on new data. As defined by Breiman [42], RF involves several key steps:

Bootstrap Aggregating (Bagging): RF creates multiple decision trees using a technique called bootstrap aggregating, or bagging. In bagging, different subsets of the training data are randomly selected with replacement to train each tree. This process ensures that each tree in the forest is a bit different from the others, which increases the diversity of the model and helps to reduce overfitting.

Decision Trees: Each decision tree in the forest makes a prediction. These trees are grown to their maximum size without pruning, which means they can capture complex patterns in the data. However, because each tree is trained on a different subset of the data and due to the randomness introduced in the selection of features at each split, the trees are less likely to overfit.

Random Feature Selection: When splitting a node during the construction of a tree, Random Forest randomly selects a subset of the features rather than using all features. This randomness helps in making the trees more diverse and leads to better generalization.

Aggregation of Predictions: Once all the trees in the forest have made their predictions, RF combines these predictions. For regression problems, this is typically done by averaging the predictions of all the trees. For classification problems, a majority voting system is used, where the final prediction is the class that receives the most votes from the trees.

6.2.2 Model Training and Testing

The RF model was designed to predict bedrock elevation *(ZZ_EPS)* in the southern GB area. Training was conducted using a subset of data from a well-constrained domain with similar geological and geographical characteristics to the target area. The dataset was converted into vector points centered on each pixel of the raster data. Since no direct measurements exist in the southern region, RF

enables extrapolation beyond the observed dataset by using spatial dependencies between selected features.

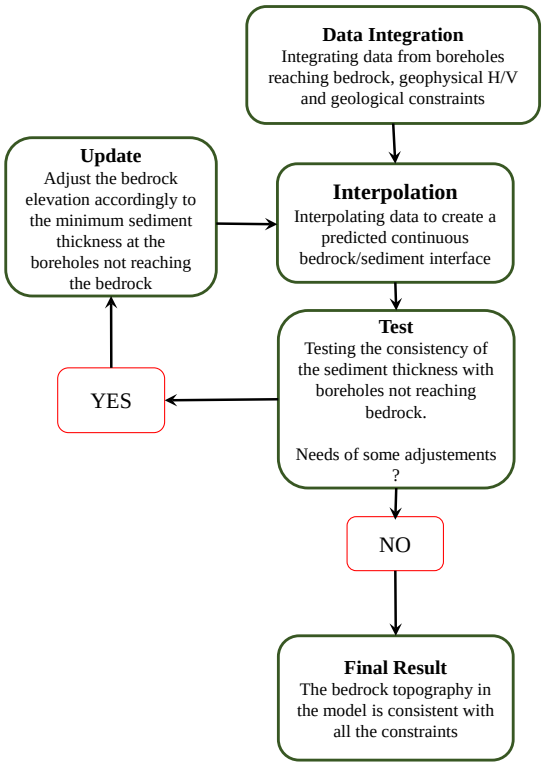

Fig. 10 Flowchart illustrating the iterative modeling methodology for bedrock elevation in GB.

To ensure reliable evaluation, the dataset was split into 80% training data and 20% testing data. The training and testing data split is represented in Fig. 12a, where blue points indicate training data and red points represent testing data. The features used to predict *ZZ_EPS* included geographical coordinates (Longitude as XX and Latitude as YY in UTM36N), distance to the coast (DC), and distance to mountains (DM). These features were chosen based on their relevance in controlling bedrock elevation within Greater Beirut's geological framework.

6.2.3 Performance Evaluation

The performance of the RF model was assessed using several metrics. Fig. 12b presents a scatter plot comparing predicted and actual bedrock elevations, demonstrating the model's precision. The data points align closely with the line of perfect prediction, illustrating that the RF model provides accurate predictions of bedrock elevation. Additionally, the model's performance was evaluated using statistical metrics. The Mean Absolute Error (MAE) of approximately 1.02 m reflects the average magnitude of prediction errors, indicating how much predictions deviate from true values on average. The Mean Squared Error (MSE) of 2.55 averages the squared differences between predictions and actual values, giving more weight to larger errors. A lower MSE indicates fewer large deviations, meaning the model minimizes significant errors effectively. The R^2 score of 0.99 represents the proportion of variance in bedrock elevation explained by the model. Since a value close to 1 indicates strong predictive accuracy, this confirms the model's reliability in estimating bedrock depth. These performance metrics are summarized in Fig. 12c.

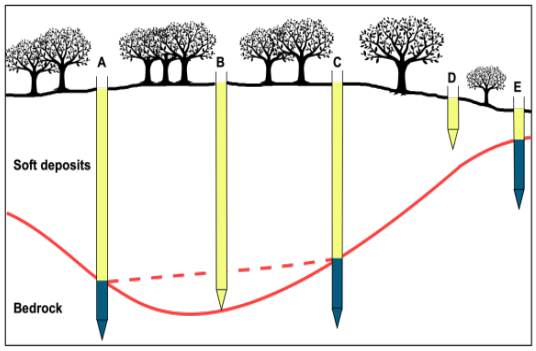

Fig. 11 Comparison of predicted bedrock elevation with minimum sediment depths from boreholes that do not reach bedrock.

7. RESULTS

7.1 3D Bedrock Elevation Model

The 3D geotechnical model of Greater Beirut provides a comprehensive visualization of bedrock elevation across the region, spanning an area of 10 km by 12 km with a 10-meter resolution, resulting in 1,225,000 cells that capture detailed elevation variations (Fig. 13). The model was generated using QGIS with the QGIS2threejs plugin and includes a primary 3D plot that highlights key topographical features, such as Beirut Port, Ras Beirut, and the surrounding mountainous terrain

In this visualization, the surface topography is represented in green, while the bedrock topography is shown in brown. Areas where the bedrock is exposed—where the two layers intersect—are clearly visible. A vertical exaggeration of 5 is applied to emphasize topographical differences, making features like mountainous terrain and coastal plains more discernible.

An inset map provides a closer view of bedrock elevation variability at a 10-meter pixel resolution. This plot highlights significant elevation changes across Greater Beirut, with steep gradients in the eastern and southern sections that reflect the mountainous terrain and gradual declines toward the western and northern coastal areas. The z-axis ranges from 0 to over 600 meters, showcasing the variation in elevation.

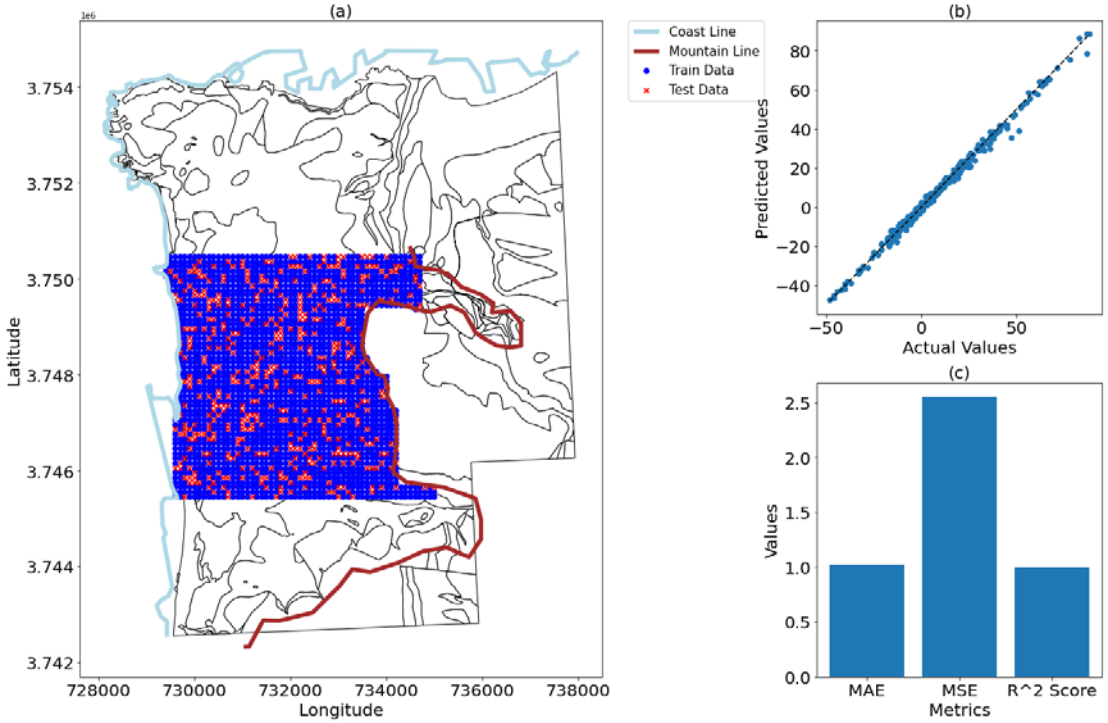

Fig. 12 (a) Training and testing data split for RF model evaluation. (b) Model performance metrics for bedrock elevation prediction. (c) Scatter plot comparing predicted and actual bedrock elevations.

The model reveals that the lowest bedrock elevation, at -74 meters, is located approximately 717 meters from the northern coast at coordinates (735461.60, 3753520.68) near Borj Hammoud and the Port of Beirut. In contrast, the highest elevation of 674 meters is situated around 8662 meters from the coast at coordinates (738050.83, 3742893.04). The eastern and southern sections exhibit steep elevations, consistent with mountainous terrain, while the western and northern areas gradually decline, reflecting a transition from highlands to coastal plains. Central regions display varied elevations, capturing the complexity of urban and natural landscapes in the region.

These topographical patterns have significant implications on seismic ground motion. Elevated areas in the south and east are likely to amplify seismic waves due to their terrain characteristics, while coastal depressions and basins may trap seismic energy, potentially intensifying ground motion in those regions.

7.2 Sediment Thickness

The sediment thickness map of Greater Beirut (GB) reveals the distribution of sediment deposits across the region, highlighting significant variations in thickness across key geographical areas (Fig. 14a). Landmarks such as Beirut Port, Beirut Airport, Haret Hreik, Borj Hammoud, Lebanese University Hadat Campus, Borj El Brajneh, Choueifat, Jnah, Ras Beirut, Achrafieh, and Furn El Chebbak are annotated alongside the Mediterranean coastline, cross-sections AA' and BB', temporary seismic stations, and borehole locations. The temporary seismic stations are represented as blue triangles on the map, and they include SERL, MTSA, CNRS, MEEL, CERD, JDE1, and ECPT.

This map highlights significant variations, with the highest sediment accumulation observed near Beirut Port, exceeding 70 meters. This thick sediment layer is likely due to littoral sand deposits, as identified in Dubertret's 1944 map. Central areas such as the Hippodrome and Furn El Chebbak also exhibit substantial sediment thickness, up to 60 meters, influenced by the alluvial deposits.

In contrast, regions like Jnah show intermediate sediment thickness ranging from 20 to 50 meters, possibly due to the sand dunes migration from the south. The Beirut Airport area shows lower sediment accumulation, between 0 and 20 meters. Achrafieh and Ras Beirut, with sediment thicknesses of less than 5 meters, align with their identification as rock sites with minimal sediment accumulation.

7.3 Cross-Sectional Analysis

To further analyze sediment distribution, cross-sections AA' and BB' were generated, as shown in Fig. 14b and Fig. 14c.

7.3.1 Cross-Section AA'

Cross-section AA' (Fig. 14b) begins at an elevation of -14 meters with a sediment thickness of 13 meters. As it progresses, the cross-section traverses varying elevations and sediment thicknesses, reaching a maximum sediment thickness of 78 meters at a distance of 1466 meters. It spans the Quaternary sedimentary basins of Greater Beirut, including areas with significant sediment thickness variations. A notable feature is the Beirut River, where a pronounced depression aligns with a thick sediment accumulation, likely influenced by fluvial transport and deposition. The bedrock surface dips sharply, forming a valley-like structure, suggesting long-term river incision and erosion. The section also passes through three of the deepest sediment deposits (basins) in the region, but a marked discontinuity is observed, possibly due to a lack of geotechnical boreholes defining sediment depth in this area. This section serves as a reference for our future numerical simulations, which will explore lithological site effects influencing ground motion amplification across various sediment layers.

The cross-section integrates borehole and geophysical data as vertical lines for guiding the interpolation process and ensuring that the model reflects subsurface conditions. Boreholes that reach bedrock (yellow lines) are considered the most reliable data points, as they provide direct physical measurements of the subsurface. Boreholes that do not reach bedrock (red lines) offer constraints on the minimum sediment thickness, while geophysical measurements (light blue lines), provide additional estimates of bedrock depth. However, these geophysical data points, which are projected onto the cross-section from distances up to 170 meters from the section line, are treated with consideration due to their interpretive nature.

In constructing the model, kriging interpolation was employed, integrating both borehole data and geophysical H/V measurements, with a preference given to data points within 100 meters of each other. In regions where boreholes do not reach bedrock, the kriging interpolation respects the minimum sediment thickness constraints, preventing the model from unrealistically reducing sediment thickness. Where both boreholes reaching bedrock and HVSR points are available within 100 meters, the kriging interpolation integrates these datasets smoothly, respecting the direct measurements from boreholes while also considering the insights provided by H/V data. For instance, in the central portion of the cross-section, where both data types are present, the model ensures a balanced approach, enhancing the reliability of the interpolated surface.

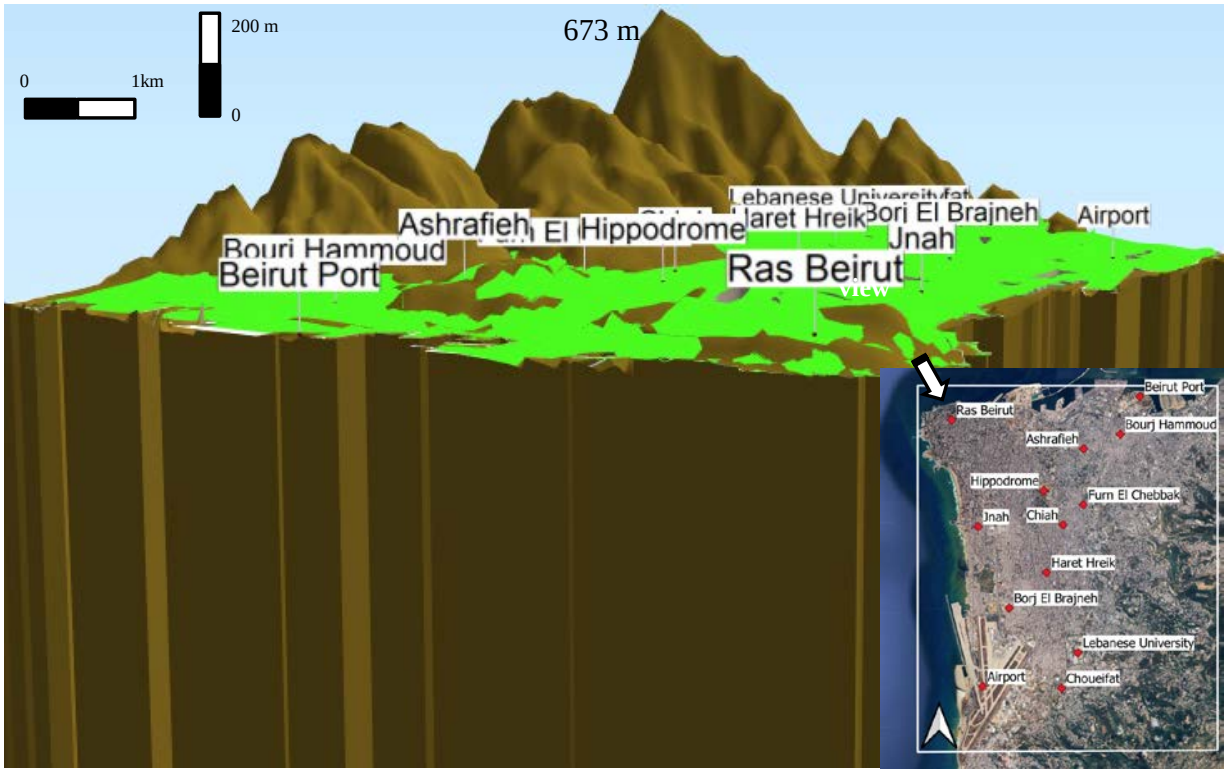

Fig. 13 3D visualization of Greater Beirut's geotechnical model. Bedrock is shown in brown, and sediments are represented in green. Key landmarks, such as Beirut Port and Ras Beirut, are highlighted. A vertical exaggeration of 5 emphasizes topographical variations, with an inset showing a detailed map and aerial perspective.

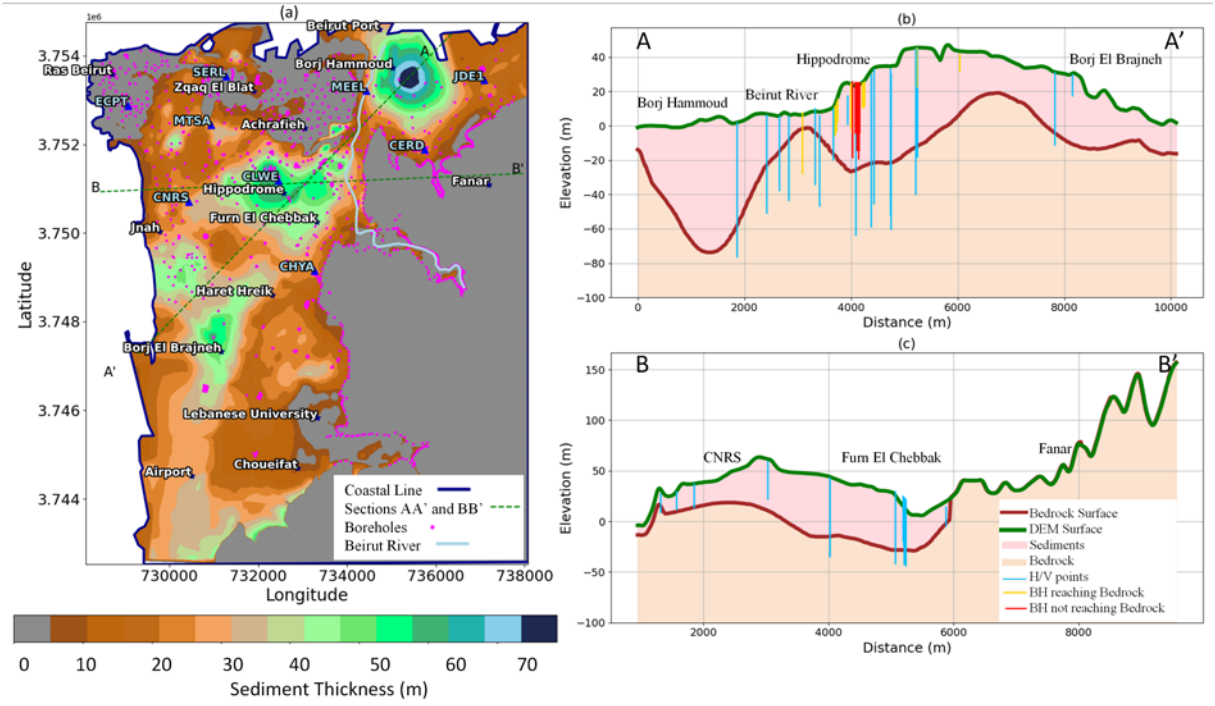

Fig. 14 (a) Sedimentary thickness map of Greater Beirut ranging from 0 meters (gray) to 80 meters (blue-gray). The coastal lines (blue), cross-sections AA' and BB' (green dashed lines), borehole locations (pink dots), temporary seismic stations (blue triangles) and the Beirut River are also shown. (b) Cross-section AA' is highlighting the deepest sediment deposits and their discontinuities. (c) Cross-section BB' illustrating the transition from coastal to mountainous terrain and associated sediment deposits.

However, in areas with sparse data, the kriging interpolation's reliability diminishes. The model becomes more dependent on the variogram assumptions, which may not fully capture the local geological variability. This is particularly evident in large sediment basins, where sparse borehole data and more distantly located H/V points allow the interpolation to vary more freely, potentially leading to less accurate representations of bedrock depth and sediment thickness. Discontinuities in the interpolated surface, especially where there are significant gaps between boreholes or transitions between different data types, highlight these limitations.

To maintain a generalized model applicable across the entire area, we avoided overfitting to the available data. Consequently, in some regions, particularly in the central portion of the section, the interpolation does not precisely follow the H/V points. This approach aligns with our global and local interpolation strategy, where the distribution of the points on the variogram (Fig. 7) explains some discrepancies in capturing finer geological details.

Additionally, when analyzing Fig. 5a, the distribution of H/V and borehole points revealed outliers beyond the standard deviation limits of the chosen mean *Vs_m* value. These deviations highlight the challenge of achieving a perfect fit between interpolated surfaces and H/V data.

Furthermore, the deviation of the interpolation from H/V and borehole data, particularly near Borj Hammoud, the Beirut River, and the Hippodrome, is also influenced by the second direction of the section. In this transitional area, extending from the Borj Hammoud through the Beirut River to Hippodrome the interpolation is constrained by two outcropping rock formations present in the perpendicular direction. These geological boundaries affect the subsurface structure, further shaping the interpolation trajectory..

7.3.2 Cross-Section BB'

Cross-section BB' (Fig. 14c) was selected to cover the transition from the Quaternary sedimentary basins to the mountainous regions in the east, where rapid elevation changes significantly influence seismic wave propagation This section starts at an elevation of -21 meters with a sediment thickness of 3 meters, and it shows significant variation in both elevation and sediment thickness as it progresses. The maximum sediment thickness observed is 62 meters at a distance of 3753 meters, with the section reaching an elevation of 158 meters and a sediment thickness of -2.25 meters by the end.

The analysis of H/V (Horizontal-to-Vertical Spectral Ratio) points along this section reveals a generally good alignment between the kriging interpolation and the H/V data, with an average difference of -0.50 meters. However, the kriging model shows variability, underestimating sediment thickness by up to 19.81 meters in some areas and overestimating it by up to 19.48 meters in others. These discrepancies suggest that while the model captures the overall sediment distribution, it may require refinement in regions with complex geology or sparse data. To improve the accuracy of the model, particularly in areas where significant deviations are observed, additional borehole data or more detailed geophysical data points or surveys could be beneficial. This would help better constrain the interpolation and reduce uncertainties in the sediment thickness estimates along section BB'.

8. DISCUSSION

8.1 Sediment Thickness Variability

The map provided in Fig. 14 illustrates the sediment thickness variability in the Beirut region, highlighting distinct green basins near Borj Hammoud, Jnah, and Furn El Chabbak. Notably, the Furn El Chabbak basin, along with the Hippodrome region, was previously identified as containing deep sediments in earlier studies [24-28]. These green areas, representing zones with thicker sediment layers, show discontinuity, raising questions about the connectivity of these sediment basins towards the western coastal areas (Fig. 14).

.While the current dataset has inherent limitations, particularly in areas with sparse borehole data, it is also possible that the basins are continuous and much deeper than indicated by our data. The existing boreholes may not adequately constrain the full extent of these basins. Future efforts should focus on increasing the density of measurement points and improving data integration to resolve these ambiguities. Enhanced data coverage will provide a clearer picture of the basin structures and their connections, leading to more accurate geological and geotechnical models. Moreover, sediment thickness discrepancies were observed in the sea area, where our model shows less constrained results. This can be attributed to the absence of direct measurement data in these regions, resulting in higher uncertainties.

8.2 Comparing Frequency Map with Previous Studies

After interpolating the sedimentary thickness as defined in Fig. 14, all points of the model grid have a defined shear wave velocity *(Vs)* of 300 m/s and a defined sedimentary thickness. This helped us estimate the 1D fundamental resonance frequencies by using Nakamura's equation, which relates these two parameters. From this estimation, we interpolated using Inverse Distnace Weight (IDW) between these grid points to reach a new interpolated frequency map. Fig. 15 presents the fundamental frequencies related to our numerical model in Beirut and its suburbs. The resonance frequency in the zones modeled as outcropping rock is fixed to 50Hz as can be seen in purple where the ECPT and SERL seismological stations are located, in Ras Beirut and Zqaq El Blat. This interpolated map reveals low to moderate fundamental frequency regions. In a previous study by Brax [24], the fundamental frequencies of measurement points obtained in Beirut, show strong correlations with the geological structures. Brax [24] identifies four low fundamental frequency regions (f_0 < 1.5 Hz): Antelias, Borj Hammoud on the eastern side of the Beirut river, and Furn El Chebbak, and Jnah, on the western side indicating thick sediment deposits in these areas. The rocky sites like Ras Beirut and Achrafieh hills display flat curves or high frequencies that were automatically fixed to 20 Hz (Fig. 2).

The frequency map derived from our model looks similar to the one of Brax [24]. The shape of the lower frequency zones is quite the same. For Borj Hammoud, the current analysis shows a frequency of 1.5 Hz, closely aligning with previous findings of low fundamental frequencies indicative of thick sediment deposits [24]. Furn El Chebbak is similarly consistent between the studies, with the current analysis identifying a frequency of 1.4 Hz, matching earlier observation of low fundamental frequencies [24].

The main differences are located on the north coast where the port area is considered as a rock site, extended north from Achrafieh hill, in our model, neglecting the artificial embankments, when Brax [24] shows a resonance frequency above 8Hz. Same can be seen north of Ras Beirut. Still, our model refines the shape and contour of the sedimentary infill compared to the model of Brax [24] by taking advantage of the complementarity between geotechnical borehole data and geophysical data.

9. CONCLUSIONS

This study presents the first comprehensive yet simplified 3D geotechnical model of Greater Beirut, developed to enhance seismic ground motion prediction beyond traditional 1D and 2D approaches. The model integrates approximately 500 geotechnical boreholes, 700 geophysical measurements, and existing geological data. To address data gaps, particularly in southern Beirut, we employed Artificial Intelligence (AI) techniques, improving the model's accuracy in regions with sparse data.

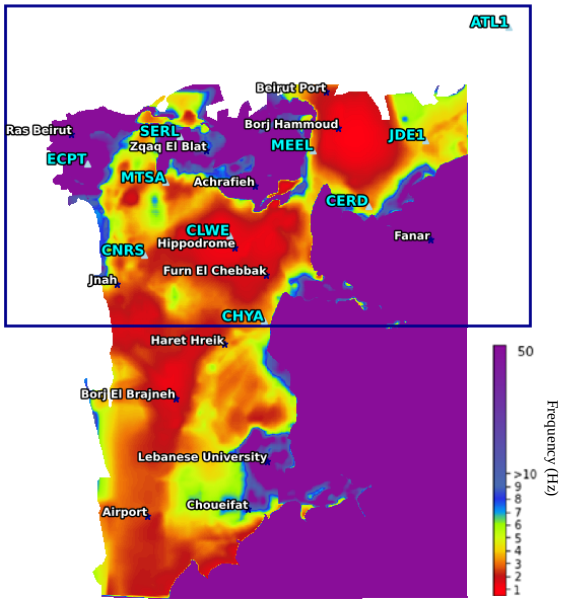

Fig. 15 Fundamental resonance frequency map of GB overlaid by temporary seismic station (light blue triangles), and the area covered (dark blue rectangle) in previous studies by Brax [24].

For shear wave velocity *(Vs)* estimation in the sedimentary layers, we combined geophysical data from H/V measurements with geotechnical data from borehole logs that reach bedrock. Using the quarter wavelength approach, we estimated an average *Vs* of 300 m/s across the model area. Due to challenges with sediment thickness data, we shifted to using bedrock elevation for interpolation, which followed a normal distribution and significantly improved the effectiveness of the Ordinary Kriging (OK) method. We also employed an iterative interpolation methodology, using boreholes that do not reach bedrock to guide the process and validate the surface for each iteration. To further refine the model, particularly in data-deficient areas of southern Beirut, we applied Random Forest (RF) methods. This allowed us to use the unique geographical features of Greater Beirut—positioned between the coast and mountains—as inputs to enhance the interpolation results.

The developed 3D model will serve as the foundation for future numerical simulations to assess site effects in the Greater Beirut, characterized by a diverse distribution of building heights and the increasing trend of vertical densification.

Moreover, although the current model uses a single sediment layer with a median *Vs_m* value, future simulations will incorporate random variability to account for small-scale subsurface heterogeneities, following the methodology proposed by [43]. This will further provide a more accurate assessment of seismic site effects in Greater Beirut.

10. ACKNOWLEDGMENTS

This This material is based on work supported by the Agence Universitaire de la Francophonie (AUF) and the CNRS-L in Lebanon as well as the PHC CEDRE program, which provided essential financial aid for the completion of this work. The authors would like also to extend their acknowledgments to the remote sensing center of the CNRS-L for supplying the Digital Elevation Model (DEM) that formed a foundation for our analysis. We are also deeply appreciative of the RUMMRE team for providing the drilling borehole data, which significantly enriched our study.

Furthermore, we acknowledge the support and collaboration of various geotechnical companies, whose expertise and provision of detailed geotechnical data were important in the development of our 3D geotechnical model. Their contributions have greatly enhanced the robustness and reliability of our findings.

11. REFERENCES

[1] Ghofrani, H., Atkinson, G.M. and Goda, K. Implications of the 2011 M9.0 Tohoku Japan earthquake for the treatment of site effects in large earthquakes. Bull Earthquake Eng 11, 2013, pp. 171–203. https://doi.org/10.1007/s10518-012-9413-4

[2] Bard P.Y. and Riepl-Thomas, J. Wave propagation in complex geological structures and their effects on strong ground motion. Wave motion in earthquake engineering, 2000, pp.37-95.

[3] Thompson E.M, Baise L.G., Tanaka Y. and Kayen R.E. “A taxonomy of site response complexity”. Soil Dynamics and Earthquake Engineering, 41, 2012,pp. 32-43. https://doi.org/10.1016/j.soildyn.2012.04.005

[4] Kaklamanos J and Bradley B.A. “Challenges in predicting seismic response with 1D analyses: Conclusions from 114 KiK-net vertical seismometer arrays”. Bulletin of the Seismological Society of America, 108(5A), 2018, pp. 2816-2838. https://doi.org/10.1785/0120180062

[5] Pilz M. and Cotton F. “Does the 1D assumption hold for site response analysis? A study of seismic site responses and implications for ground motion assessment using KiK-net strong-motion data”. Earthquake Spectra, 35(2), 2019, pp. 883-905. https://doi.org/10.1193/050718EQS113M

[6] Afshari K. and Stewart J.P. “Insights from California vertical arrays on the effectiveness of ground response analysis with alternative damping models”. Bulletin of the Seismological Society of America, 109(4), 2019, pp. 1250-1264. https://doi.org/10.1785/0120180292

[7] Pitarka, A., Irikura, K., Iwata, T., & Sekiguchi, H.

Three-dimensional simulation of the near-fault ground motion for the 1995 Hyogo-ken Nanbu (Kobe), Japan, earthquake. Bulletin of the Seismological Society of America, 88(2), 1998, pp.428-440.

[8] Bard, P.-Y., & Bouchon, M. The two-dimensional resonance of sediment-filled valleys. Bulletin of the Seismological Society of America, 75, 1985, pp. 519-541.

[9] Bard, P.-Y. and Bouchon, M. The seismic response of sediment-filled valleys. Part I. The case of incident SH waves, Bull Seismol Soc Am, 70, 1980a, pp. 1263-1286.

[10] Bard, P.-Y. and Bouchon, M. The seismic response of sediment-filled valleys. Part II. The case of incident P and SV waves, Bull Seismol Soc Am, 70, 1980b, pp.1921-1941.

[11] Kawase, H. The cause of the damage belt in Kobe: "The basin-edge effect," constructive interference of the direct S-wave with the basin-induced diffracted/Rayleigh waves. Seismological Research Letters, 67(5), 1996, pp.25-35.

[12] Tsuno, S. E. Chaljub and P.-Y. Bard. Grenoble simulation benchmark: comparison of results and main learnings. ESG2006 Proceedings, Edited by P.-Y. Bard, E. Chaljub, C. Cornou, F. Cotton and P. Guéguen, LCPC Editions, ISSN 1628-4704, Vol.2, 2009, pp. 1377-1436.

[13] Thompson, M., Wirth, E.A., Frankel, A.D., Hartog, J.R. and Vidale, J.E. Basin amplification effects in the Puget Lowland, Washington, from strong-motion recordings and 3D simulations. Bulletin of the Seismological Society of America, 110(2), 2020, pp.534-555.

[14] Sadek, S., Harajli, M. and Asbahan, R. A GIS-based framework for the evaluation of seismic geo-hazards in the greater Beirut area. 11th international conference on soil dynamics and earthquake engineering and the 3rd international conference on earthquake geotechnical engineering Proceedings, University of California, Berkley. 2004, pp. 89-96.

[15] Antonielli B., Iannucci R., Ciampi P., Govoni A., Romano A., Engineering-geological modeling for supporting local seismic response studies: insights from the 3D model of the subsoil of Rieti (Italy), Bulletin of Engineering Geology and the Environment, Vol. 82, Article 235, 2023. https://doi.org/10.1007/s10064-023-03259-4

[16] Petrone P., Allocca V., Fusco F., Romagnoli G., Engineering geological 3D modeling and geotechnical characterization in the framework of technical rules for geotechnical design: the case study of the Nola's logistic plant (southern Italy), Bulletin of Engineering Geology and the Environment, Vol. 82, Article 12, 2023. https://doi.org/10.1007/s10064-022-03017-y

[17] Dong M., Neukum C., Hu H., Azzam R., Real 3D geotechnical modeling in engineering geology: A case study from the inner city of Aachen, Germany, Bulletin of Engineering Geology and the Environment, Vol. 74, 2015, pp. 281-300.

[18] El Houssainy A., Abi-Ghanem C., Dang D., Mahfouz C., Omanović D., Khalaf G., Mounier S., Garnier C., Distribution and diagenesis of trace metals in marine sediments of a coastal Mediterranean area: St Georges Bay (Lebanon), Marine Pollution Bulletin, Vol. 155, 2020, 111066. https://doi.org/10.1016/j.marpolbul.2020.111066

[19] Shiber J., Metal concentrations in marine sediments from Lebanon, Water, Air, and Soil Pollution, Vol. 13, 1980, pp. 35-43. https://doi.org/10.1007/BF02262523

[20] Daëron M., Klinger Y., Tapponnier P., Elias A., Jacques E., Sursock A., 12,000-year-long record of 10 to 13 paleoearthquakes on the Yammouneh fault, Levant fault system, Lebanon, Bulletin of the Seismological Society of America, Vol. 97, No. 3, 2007, pp. 749-771. https://doi.org/10.1785/0120060106

[21] Elias A., Tapponnier P., Singh S.C., King G.C., Briais A., Daëron M., Carton H., Sursock A., Jacques E., Jomaa R., Klinger Y., Active thrusting offshore Mount Lebanon: Source of the tsunamigenic AD 551 Beirut-Tripoli earthquake, Geology, Vol. 35, No. 8, 2007, pp. 755-758. https://doi.org/10.1130/G23631A.1

[22] Walley C.D., A braided strike-slip model for the northern continuation of the Dead Sea Fault and its implications for Levantine tectonics, Tectonophysics, Vol. 145, Issues 1-2, 1988, pp. 63-72. https://doi.org/10.1016/0040-1951(88)90316-2

[23] El Kadri S., Beauval C., Brax M., Bard P.Y., Vergnolle M., Klinger Y., A fault-based probabilistic seismic hazard model for Lebanon, controlling parameters and hazard levels, Bulletin of Earthquake Engineering, 2023, 35p. https://doi.org/10.1007/s10518-023-01631-z. hal-04031004

[24] Brax M., Bard P.Y., Duval A.M., Bertrand E., Rahhal M.E., Jomaa R., Cornou C., Voisin C., Sursock A., Towards a microzonation of the Greater Beirut area: an instrumental approach combining earthquake and ambient vibration recordings, Bulletin of Earthquake Engineering, Vol. 16, 2018, pp. 5735–5767. https://doi.org/10.1007/s10518-018-0438-1

[25] Salloum N., Jongmans D., Cornou C., Abdel Massih D. Y., Hage Chehade F., Voisin C., Mariscal A., The shear wave velocity structure of the heterogeneous alluvial plain of Beirut (Lebanon): combined analysis of geophysical and geotechnical data, Geophysical Journal International, Vol. 199, No. 2, 2014, pp. 894-913.

https://doi.org/10.1093/gji/ggu294

[26] Brax M., Causse M., Bard P.Y, Ground motion prediction in Beirut: a multi-step procedure coupling empirical Green's functions, ground motion prediction equations and instrumental transfer functions, Bulletin of Earthquake Engineering, Vol. 14, 2016, pp. 3317-3341. https://doi.org/10.1007/s10518-016-0004-7

[27] Atwood A., West A.J., Evaluation of high‐resolution DEMs from satellite imagery for geomorphic applications: A case study using the SETSM algorithm, Earth Surface Processes and Landforms, Vol. 47, No. 3, 2022, pp. 706-722. https://doi.org/10.1002/esp.5263

[28] Dubertret. Géologie du site de Beyrouth avec carte géologique au 1/20.000 et 9 planches (56 pages), 1944. Délégation Générale de France au Levant, Section géo-logique, Beyrouth.

[29] QGIS Development Team, QGIS Geographic Information System (Version 3.30's-Hertogenbosch) [Software]. Open Source Geospatial Foundation, 2023. https://www.qgis.org

[30] Ibrahim E., Massih D.Y.A., Harb J., An investigation of Beirut soil properties. 2nd International Conference on Advances in Computational Tools for Engineering Applications (ACTEA), Beirut, Lebanon, 2012, pp. 186-191. https://doi.org/10.1109/ICTEA.2012.6462863

[31] Nakamura Y., A Method for dynamic characteristics estimation of subsurface using microtremor on the ground surface, Quarterly Report of RTRI (Railway Technical Research Institute), Vol. 30, 1989, pp. 25–33.

[32] Supriyadi K.S., Fadilah, A. R., and Muttaqin, W.H. Study of the Subsurface Structure Based on Microseismic Data in the Heritage Area of Kota Lama Semarang, Indonesia. International Journal of GEOMATE, 23(97) 2022, pp.211-219. https://doi.org/10.21660/2022.97.j2357.

[33] Prasetya, A. R., Faris, F. and Rahardjo, A. P. Seismic Vulnerability Assessment Using the HVSR Method at Yogyakarta International Airport Underpass, Indonesia. International J. of GEOMATE, 26(114), 2024, pp.25-33. https://doi.org/10.21660/2024.114.4082

[34] Nakamura Y. Clear identification of fundamental idea of Nakamura's technique and its applications. In Proceedings of the 12th world conference on earthquake engineering, vol. 2656, 2000, pp. 1-8.

[35] Walsh L. Digital Topography: Should you choose a TIN or raster interpolation of the landscape. The University of Maryland, Geology Department, 2017, pp. 1-4. https://serc.carleton.edu/48146.

[36] Webster, R. and Oliver, M.A. Geostatistics for environmental scientists. John Wiley & Sons, 2007, pp. 1-315. ISBN-13: 978-0-470-02858-2.

[37] Oliver M.A., Webster R., A Tutorial guide to geostatistics: Computing and modelling variograms and kriging, Catena, Vol. 113, 2014, pp. 56-69. https://doi.org/10.1016/j.catena.2013.09.006

[38] Guo-Shun L., Hou-Long J., Shu-Duan L., Xin-Zhong W., Hong-Zhi S., Yong-Feng Y., Xia-Meng Y., Hong-Chao H., Qing-Hua L., Jian-Guo G., Comparison of kriging interpolation precision with different soil sampling intervals for precision agriculture, Soil Science, Vol. 175, No. 8, 2010, pp. 405-415. https://doi.org/10.1097/SS.0b013e3181ee2915

[39] Legleiter C.J., Kyriakidis P.C., Spatial prediction of river channel topography by kriging, Earth Surface Processes and Landforms, Vol. 33, No. 6, 2008, pp. 841-867. https://doi.org/10.1002/esp.1579

[40] Vieira, S.R., Carvalho, J.R.P.D., Ceddia, M.B. and González, A.P. Detrending non stationary data for geostatistical applications. Bragantia, 69, 2010, pp.01-08.

[41] Young C., Kushnereit S. Beal R., Yan, T. T. L., and Pham, H. Application of geostatistical techniques to quantify changes in water levels. Report for Victoria County Groundwater Conservation District, 2021, pp. 1-64.

[42] Breiman L., Random Forests, Machine Learning, Vol. 45, 2001, pp. 5-32. https://doi.org/10.1023/A:1010933404324

[43] Tchawe, F.N., Gelis, C., Bonilla, L.F. and Lopez-Caballero, F. Effects of 2-D random velocity perturbations on 2-D SH short-period ground motion simulations in the basin of Nice, France. Geophysical Journal International, 226(2), 2021, pp.847-861.